Ann. Geophys., 27, 2585–2592, 2009
www.ann-geophys.net/27/2585/2009/

Annales Geophysicae

F-region electron heating by X-mode radiowaves in underdense conditions

H. Löfås[1,2], **N. Ivchenko**[2], **B. Gustavsson**[3], **T. B. Leyser**[4], **and M. T. Rietveld**[5]

[1]Uppsala University, Uppsala, Sweden
[2]Space and Plasma Physics, School of Electrical Engineering, KTH, Stockholm, Sweden
[3]Univ Tromsø, Dept Phys & Technol, 9037 Tromsø, Norway
[4]Swedish Institute of Space Physics, Uppsala, Sweden
[5]EISCAT, 9027 Ramfjordbotn, Norway

Received: 28 November 2008 – Revised: 5 June 2009 – Accepted: 16 June 2009 – Published: 26 June 2009

Abstract. Observations of modifications of the electron temperature in the F-region produced by powerful high frequency radiowaves at 4.04 MHz transmitted in X-mode are presented. The experiments were performed during quiet nighttime conditions with low ionospheric densities so no reflections occurred. Electron temperature enhancements of the order of 300–400 K were obtained. Numerical simulation of ohmic heating by the pump wave reproduces both altitude profiles and temporal dependence of the temperature modifications in the experiments.

Keywords. Ionosphere (Wave propagation) – Radio science (Ionospheric propagation; Waves in plasma)

1 Introduction

A powerful High Frequency (HF) radio wave can perturb the ionospheric plasma significantly and induce a great number of interesting plasma-physical phenomena near the reflection altitude (e.g. Gurevich, 2007, and references therein). This includes instabilities and mode conversions driving Langmuir and upper hybrid turbulence leading to large electron temperature enhancements (Honary et al., 1993; Robinson et al., 1996; Leyser et al., 2000; Rietveld et al., 2003), creation of field aligned density depletions (Kelley et al., 1995; Ponomarenko et al., 1999), acceleration of electrons (Carlson et al., 1982) and radio induced emissions at HF and optical frequencies (Bernhardt et al., 1989; Leyser, 2001; Brändström et al., 1999; Gustavsson et al., 2001; Kosch et al., 2007).

Correspondence to: N. Ivchenko
(nickolay@kth.se)

Along the entire wave propagation path there is also Ohmic heating due to non-zero HF-conductivity and associated collisional damping of the HF-wave. The Ohmic effect has been studied for overdense conditions (Shoucri et al., 1984; Hansen et al., 1992a; Hansen et al., 1992b). For such conditions most of the energy deposition in the F-region occurs just below the reflection altitude. From there heat is convected up and down along the magnetic field (Gonzalez et al., 2005; Mantas et al., 1981). Due to a large number of possible wave-plasma processes acting in the region close to the reflection altitude it is difficult to accurately separate the effects of Ohmic heating from the effects of nonlinear and resonant processes, unless one keeps the ERP (Effective radiated power) low enough to make sure the peak E-field amplitude is below the threshold for the nonlinear processes. When transmitting X-mode waves at frequencies above the critical frequency for reflection, f_XF2 there is no standing wave and only limited beam swelling. Further there is no altitude where the pump frequency is equal to the frequency of upper-hybrid resonance, f_{UH}, or the plasma frequency, f_P, and no resonances are excited. Thus underdense heating makes it possible to study the effect of Ohmic heating with large amplitude E-fields in a large altitude range.

In order to isolate the effect of Ohmic heating we performed a series of experiments at the EISCAT heating facility (Rietveld et al., 1993) between 17 and 19 October 2006 with X-mode transmission at frequencies above f_XF2. The ionospheric response of the heating was observed with the EISCAT UHF radar (Rishbeth and van Eyken, 1993). In this article we present observations of modulation of 30–40% of the electron temperature, T_e, with increases of up to 400 K. Numerical integration of the energy equation shows that the observed altitude and temporal variation can be explained by Ohmic heating.

Published by Copernicus Publications on behalf of the European Geosciences Union.

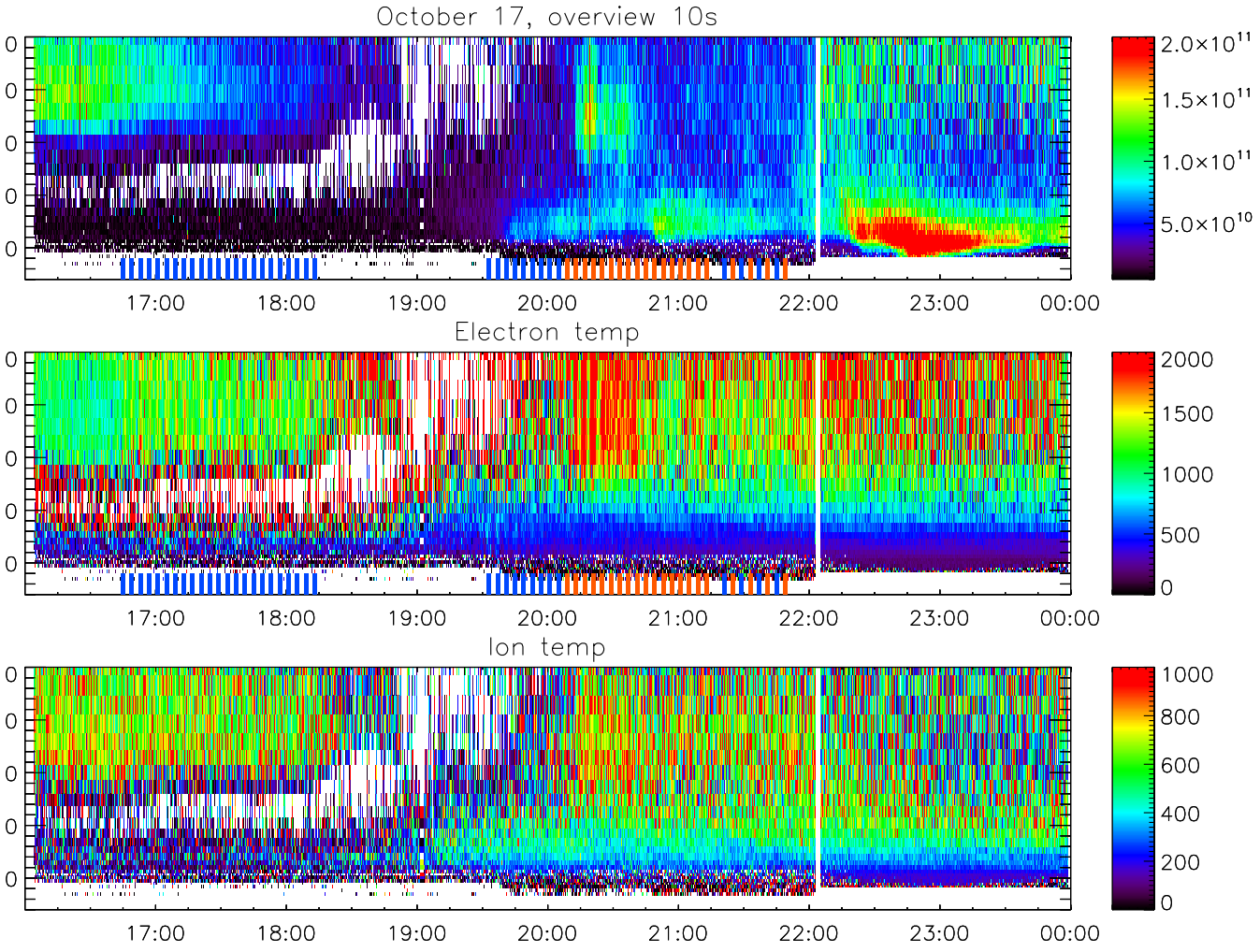

Fig. 1. Overview of the EISCAT data from 17 October 2008. Electron density (upper panel) shows a steady decrease until 19:00 UT while T_e (middle panel) is modulated by the HF-transmission, no significant change is seen in T_i (lower panel). The bars under the plots indicate when the heater facility was running: blue bars indicate X-mode and red bars O-mode

Although there have been predictions and indirect deductions of temperature enhancements caused by X-mode heating, to our knowledge there is only one other publication with observations of X-mode temperature enhancements in the F-region. Showen and Behnke (1978) briefly mention that only rarely has X-mode heating succeeded and only in the reflection case with a maximum change of 100K.

2 Experiments and observations

Three evening experiments with transmission in the magnetic zenith at 4.04 MHz were run with the EISCAT Heating facility (located at 69.6° N, 19.2° E outside Tromsø, northern Norway) on 17, 18 and 19 October 2006. The ionospheric response was observed with the EISCAT UHF incoherent scatter radar also pointed in the direction of the magnetic zenith.

Modulations of the F-region electron temperature, T_e, were found even though the peak plasma density was too low for reflection either of X- or O-mode transmission of the 4.04 MHz pump wave in all cases, but the first couple heating pulses on 19 October. There is no conspicuous difference in the electron temperatures between the first pulses and the subsequent ones, suggesting either that the ionosphere was indeed sub-critical or that the energy deposition is similar for the case with reflection near the peak of the electron density profile. In either case, the reflection effects are beyond the scope of this paper.

An overview of the modulations observed on 17 October is shown in Fig. 1. A 2 min on 2 min off cycle was used. The transmission, 180 MW ERP with an estimated D- and

Table 1. Observed and simulated parameters.

Day	$\Delta T_{\rm obs}$(K)	$t_{\rm obs}^{\rm rise}$ (s)	$t_{\rm obs}^{\rm decay}$ (s)	$\Delta T_{\rm siml}$(K)	$t_{\rm siml}^{\rm rise}$ (s)	$t_{\rm siml}^{\rm decay}$ (s)
17 Oct	370	13	7	303	10	11
18 Oct	290	23	19	376	10	11
19 Oct	420	20	7	247	10	10

E-region absorption of 5 dB, was in X-mode from 16:48 to 18:14 UT, and from 19:32 to 20:08 UT, then from 20:08 to 21:14 UT the transmission was in O-mode. The UHF radar was observing in the magnetic zenith with the tau2pl program giving an intrinsic time resolution of 5 s and a range resolution of 5 km. At the start of the experiment the peak plasma density measured by the radar was approximately $9 \times 10^{10}\,\mathrm{m}^{-3}$ which corresponds to a plasma frequency of 3.1 MHz and a f_XF2 of 4.01 MHz with the peak at 240 km, confirmed independently with ionosonde observations. The density continued to decrease during the experiment and at around 18:00 UT, with f_0F2 at 2.1 MHZ corresponding to an X-mode critical frequency of approximately 3 MHz, the signal became too low to be reliably detected by the radar.

On 18 and 19 October the conditions were similar, with peak densities below the critical value for X-mode reflection, but slightly higher than on 17 October. On 18 October the transmission was in a 2 min on 2 min off cycle between 16:40 UT and 18:42 UT in X-mode when f_0F2 decreased from 3.1 to 2 MHz corresponding to a f_XF2 decrease from 4.03 MHz to 3 MHz with the peak at 270 km. The radar was running the arc1u program during this experiment giving an intrinsic time resolution of 0.44 s and a range resolution of 0.9 km, which resulted in lower signal to noise ratio in the F-region which gives larger uncertainty in the results. Here, temperature modulation was observed throughout the heater operation. On 19 October the transmission was in a 3 min on 3 min off cycle in X-mode between 16:15 UT and 17:29 UT. The radar was running the tau2pl program. Electron temperature modulation in the F-region was also observed in this experiment as well. During the 19 October event the density decreased rapidly, and analysis of radar data gives reliable results for only five heating cycles between 16:15 and 17:00 UT when f_0F2 decreased from 3.2 to 1.5 MHz corresponding to a decrease in f_XF2 from 4.14 MHz to 2.5 MHz with the peak at 250 km.

To make a more detailed analysis of the characteristic rise and decay times of the temperature enhancements for the low-density conditions (with the accompanying poor signal-to-noise ratio) we apply conditional averaging of the decoded radar acf estimates. In order to reduce noise, and still resolve the rapid variation of the ionospheric response to the HF-transmission power on/off the autocorrelation functions received at the same offset time from the nearest HF on time were integrated together. (A similar analysis was used by Djuth et al. (2004) to characterize the initial enhancements of Langmuir turbulence upon HF turn on, and by Grydeland et al. (2008) to resolve fast variations of backscatter power related to flickering aurora). Ion and electron temperatures, which only depend on the shape of the Incoherent Scatter (IS) spectrum are accurately estimated with this analysis during stable conditions, where the T_e modulation is caused by the periodic HF-pump cycle. This gives estimates of T_e and T_i with a time resolution of 10 s for tau2pl and 8 s for arc1u with a sufficient signal to noise ratio. This time resolution is of the same order of magnitude as the thermal response studied here. The electron density obtained this way is an average over the whole period in question and is not representative, as the density decreases systematically throughout all three experiments. The integration used a range gate interval of 10 km in altitude and was performed between 200 km and 300 km.

In all three experiments the highest T_e increases are found in the 230–240 km altitude interval. The results of the conditional averaging over the periods with similar electron density profiles (16:48 UT to 18:14 UT for 17 October, 17:00 UT to 17:40 UT for 18 October and 16:15 UT to 16:45 UT for 19 October) are shown in Fig. 2. On 17 October T_e increases by approximately 370 K, on 18 October by 290 K and on 19 October by 420 K. The characteristic times and temperature increases for all three days are shown in the three first columns of Table 1, to examine the characteristic times a model of exponential increase ($a(1-e^{-t/T})+c$) and exponential cooling ($(ae^{-t/T})+c$) is fitted to the data with non-linear least squares. The rise and decay times of the modulation are in the order of ten seconds, with longer times for 18 October.

The altitude profiles of the steady state temperatures for heater on-off cycles are shown in Fig. 3. The figure shows electron temperature profiles for both heater on and heater off periods. Here the temperature has been averaged over periods when Te is reasonably stable, starting 1 min after heater on or off. In Fig. 3 it can be clearly seen that the largest increases in temperature occurs at around 230–240 km for all three days. It is also worth noting that the undisturbed temperature increases with altitude which indicates a heat flow into the ionosphere from above.

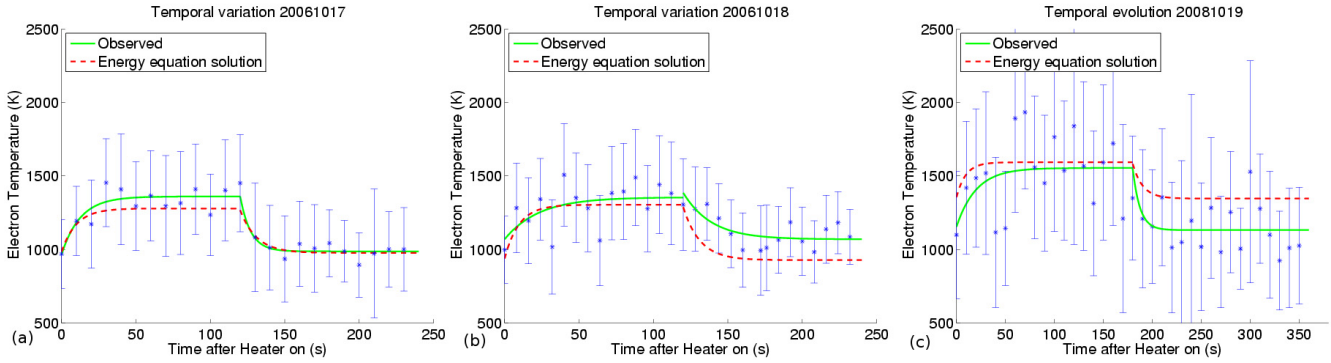

Fig. 2. Temporal evolution of the electron temperature for the three different days, **(a)** 17 October, **(b)** 18 October and **(c)** 19 October. Temperatures derived from conditionally averaged raw radar data,received at the same offset time from the nearest HF on time, are plotted vs. time along with the error bars. Exponential fits to temperature rise and fall are shown in green. Results of the time dependent modeling of collisional Ohmic heating by the pump wave are shown in red (see text).

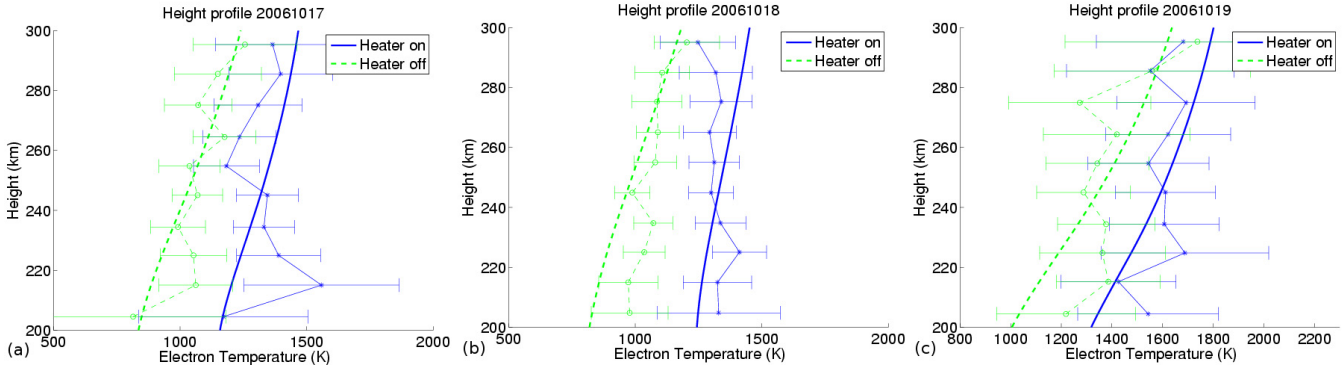

Fig. 3. Height dependence of the electron temperature for HF-on (blue) and HF-off (green), for 17 October **(a)**, 18 October **(b)** and 19 October **(c)**. Both observed profiles (thin line) and the solution of the energy equation (thick line) are shown.

3 Modeling

The ionospheric response to HF-heating on these long timescales are described by the coupled ion and electron continuity, momentum and energy equations (Banks and Kockarts, 1973; Schunk and Nagy, 1978; Shoucri et al., 1984; Hansen et al., 1992a; Hansen et al., 1992b). For the underdense conditions of our experiments, the HF-heating is smoothly distributed in altitude and there is no significant density modulation and no plasma expulsion from a region close to a reflection altitude. Our observations also show no detectable change in T_i during the HF transmission thus we can simplify the model by only considering the electron energy equation.

3.1 The model

Considering that heat conductivity is much larger along the background magnetic field than perpendicular, and that the transverse plasma drifts through the beam are slow compared with characteristic times for electron heating and cooling, we can simplify the problem further to only study the variations in one dimension, along the magnetic field. Further, field-aligned electron drifts are small, making convective terms negligible. Under these assumptions the electron energy equation can be written:

$$\frac{3}{2}n_e k_B \frac{\partial T_e(t,z)}{\partial t} = \frac{\partial}{\partial z}\left(K_e(T_e)\frac{\partial T_e(t,z)}{\partial z}\right) + Q(t,z) + Q_0(t,z) - L_e(T_e) \quad (1)$$

where Q_0 is the background sources (energy deposition from photoionisation and other sources), Q is the energy deposition by the pump wave, L_e is the rate of energy loss due to both elastic and inelastic collisions with ions and neutrals, and K_e is the parallel thermal conductivity. We use thermal conductivity from Banks and Kockarts (1973)

$$K_e = \frac{7.7\times10^5 T_e^{5/2}}{1+3.22\times10^4(T_e^2/n_e)\sum_s n_s \bar{Q}_D} \mathrm{eVcm^{-1}s^{-1}K^{-1}} \quad (2)$$

where $\bar{Q}_D$ is the average momentum transfer cross section which in the case of electron ion collisions can be written as

$$\bar{Q}_D = (\pi/2)(e^2/4\pi\epsilon_0 k_B T_e)^2 \ln\Lambda \tag{3}$$

The main electron energy loss processes are elastic collisions with ions and inelastic collisions with neutrals. The electron-ion energy transfer rate is

$$L_{e,i} = \frac{4(2\pi m_e)^{1/2}}{m_i} n_e n_i \left(\frac{z_i e^2}{4\pi\epsilon_0}\right)^2 \frac{k_B(T_e - T_i)}{(k_B T_e)^{3/2}} \ln\Lambda \tag{4}$$

where z_i is the atomic charge and the Coulomb logarithm is defined as (Schunk and Nagy, 1978)

$$\ln\Lambda = \ln\left(\frac{16\pi\epsilon_0 k_B T_e}{\gamma^2 z_i e^2 k_e}\right) - \frac{k_e^2 + k_i^2}{k_e^2} \ln\left(\frac{(k_i^2 + k_e^2)^{1/2}}{k_e}\right) \tag{5}$$

and

$$k_i^2 = \frac{n_i z_i^2 e^2}{\epsilon_0 k_B T_i} \tag{6}$$

$$k_e^2 = \frac{n_e e^2}{\epsilon_0 k_B T_e} \tag{7}$$

If the ionosphere is assumed to consist mainly of NO^+,O_2^+,O^+,He^+ and H^+ and the different ions are assumed to have equal temperature the expression for the cooling rate takes the form

$$L_{e,i} = 3.2\times10^{-14} n_e \frac{(T_e - T_i)}{T_e^{3/2}} \ln\Lambda \times \ldots \left(n_{O^+} + 4n_{He^+} + 16n_{H^+} + 0.5n_{O_2^+} + 0.53n_{NO^+}\right) \tag{8}$$

where $L_{e,i}$ is given in $\mathrm{eVm^{-3}s^{-1}}$, T_e in K and the density $n_{e,i}$ in $\mathrm{m^{-3}}$ (Schunk and Nagy, 1978).

The loss due to collisions with neutrals occurs mainly in inelastic processes exciting rotational, vibrational and atomic states in the molecules and atoms. We use the cooling rates from Pavlov (1998a,b); Pavlov and Berrington (1999). The neutral densites has been obtained from MSIS model (Hedin, 1991) for the actual day and ion densities from IRI-model.

The heat source, Q, we calculate from the ordinary expression for Joule heating (Shoucri et al., 1984)

$$Q = <\mathcal{J}\cdot\mathcal{E}> = \frac{1}{2}\mathrm{Re}\left(\boldsymbol{E}^*\cdot\boldsymbol{\sigma}\cdot\boldsymbol{E}\right) \tag{9}$$

where σ is the conductivity tensor and the wave electrical field E at altitude z is

$$E_\pm = E(z_0)\left(\frac{z_0}{z}\right)\left[\frac{\epsilon_\pm(z_0)}{\epsilon_\pm(z)}\right]^{1/4} \exp\left(ik_0\int_{z_0}^{z}\mathcal{N}_\pm(z)dz\right) \tag{10}$$

Here $\epsilon_\pm$ denotes the dielectric tensor for the X-mode (+) and O-mode (−) polarized waves, k_0 is the wave number at the bottom of the ionosphere, and finally $\mathcal{N}_\pm(z)$ is the complex refractive index. Here we use the formulas of Shoucri et al. (1984) for the conductivity and dielectric tensors and estimate the HF-pump wave E-field at the bottom of the ionosphere, $E(z_0)$, by free space propagation. Here we use $z_0 = 150$ km. Even though there is no reflection altitude some beam swelling will occur in the region where the local plasma frequency approaches the pump frequency. There the refractive index for the pump frequency decreases and leads to a reduction of phase velocity, to conserve Poynting flux the wave amplitude grows.

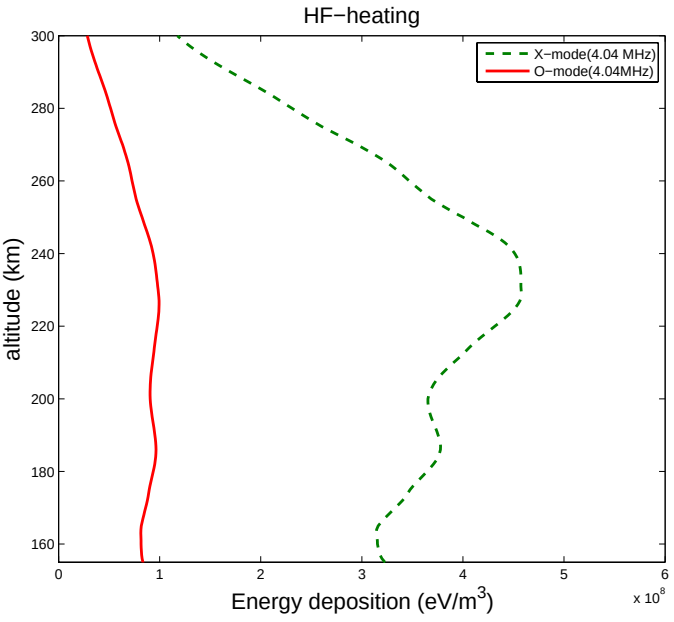

Fig. 4. Profile of X-mode energy deposition from heater used for solution of the energy equation for October 17. Calculated values for O-mode for the same frequency is shown as a comparison.

3.2 Results

Good agreement with the observed electron temperature enhancements is obtained for 17 and 19 October by numerically integrating the electron energy equation (Eq. 1) from a altitude of 180 km up to 320 km, using a Crank-Nicholson scheme with 0.1 s timestep and 3.4 km grid in altitude and Ohmic heating by the pump wave calculated using Eqs. (9) and (10). For 17 and 19 October the integration of Eq. (1) gives a good fit with the observed T_e. For 18 October we obtain a slightly higher electron temperature enhancement than is observed, shown in Fig. 2.

The calculated profile of the energy deposition for 17 October is shown in Fig. 4, where an ERP of 180 MW is used, which is a good estimate for array 2 with radiated frequency of 4.04 MHz. The beam spread is 14.5° (Rietveld et al., 1993). When integrating Eq. (1) we set the heat flux,

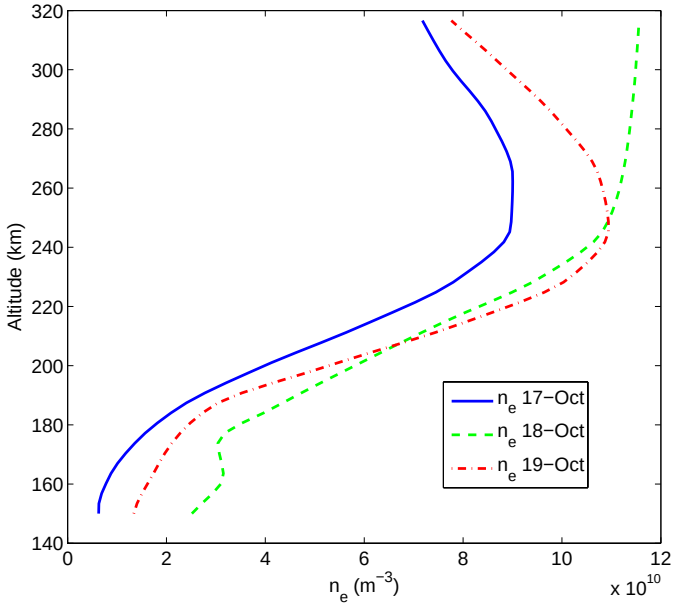

Fig. 5. Electron density profiles used for the simulations.

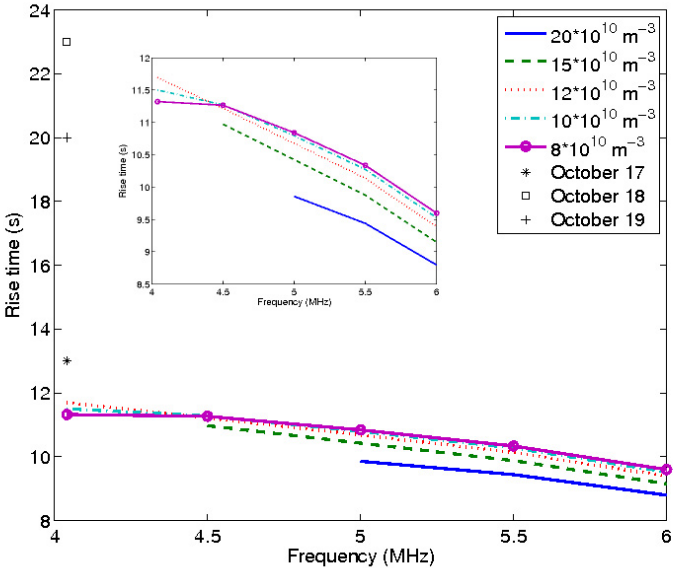

Fig. 7. Rise time as a function of heater frequency, observed values plotted as comparsion. Inset is zoomed in on modeled times.

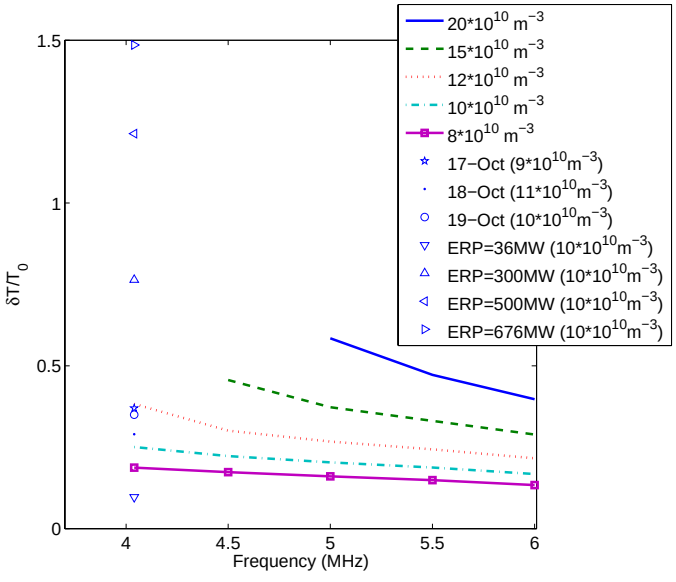

Fig. 6. Temperature increase as a function of heater frequency, observed values plotted as comparsion.

$K(T_e)\Delta T_e/\Delta z$, at the lower boundary to zero, since at that altitude local losses dominate. At the upper boundary we adjust the downward heat flux to give the best agreement with the observed unperturbed background T_e profiles. These values of the heat flux, shown in Table 2, reproduce the general behavior of the background temperature profiles, but not all of the small-scale details. These are reasonable values for the heat flow in the ionosphere (Roble and Hastings, 1977) during quiet conditions. For quiet nighttime conditions there are few ambient heat sources and the Q_0 term can be neglected in the simulation. In these conditions the background profile is determined only by heat flow at the top of the ionosphere and losses in the ionosphere.

Table 2. Heat flow used in simulation.

Day	Heat flow ($\mathrm{eVm^{-2}s^{-1}}$)
17 Oct	1.1×10^{13}
18 Oct	1.4×10^{13}
19 Oct	2.6×10^{13}

When calculating the electron loss rates we use T_i from the observations and constant neutral temperatures and density profiles from the MSIS model. The electron density profile used is filtered and smoothed from the radar data at the time of the first heating cycle shown in Fig. 5.

The reason for the higher simulated temperature enhancements could be due to the fact that the simulation is done using the electron densities observed during the first heating cycle, but the conditionally averaged T_e is an average over several cycles, with decreasing n_e. The same model used for fitting of experimental data described in the previous section is also used for describing the simulated data, results are shown in the three last columns of Table 1. One can see that the temperature increases ($\Delta T/T_{e,0}$) are in good agreement compared to observations. The rise and decay times are roughly the same but are different compared to observations. For 18 October, however, the calculation gives a significantly

larger increase in temperature than observed. For that day there is a larger electron density at low altitudes in the observed data, which indicates precipitation to lower altitudes causing larger absorption of the pump wave.

During the analysed cycles the density is continuously decreasing and when the density decreases the Ohmic energy deposition decreases faster than the cooling rates which leads to smaller temperature increases. To compare our observational results, shown in Table 1, with dependence on different heating conditions (peak electron density and heater frequency), the simulation was repeated for different heater frequencies with density profiles from 17 October scaled to different peak electron densities. These results are shown in Fig. 6, where the frequency dependence of the fractional temperature increase ($\Delta T/T_{e,0}$) is shown, and Fig. 7, which shows the dependence of the rise time on frequency. Both the temperature increase and the rise time for these figures are calculated at an altitude of 220 km. It is possible to see that the temperature increase is larger with increasing ionospheric density, and decreases with heater frequency. The characteristic times are only slightly affected, but significantly lower than our observed, increasing somewhat for lower densities and lower heater frequencies. $\Delta T/T_{e,0}$ was calculated for different ERP the electron density profile of October 17, with a low ERP of 36 MW (typical for HIPAS) and a high ERP of 676 MW (typical for HAARP) shown in Fig. 6. For the low ERP case we get a temperature increase of about 10% and for the high ERP case we get a temperature increase of almost 150% above the background profile. For comparisons with experimental observations, one should remember that these temperature estimates are for under-dense heating with a pump frequency at 4.04 MHz, and that both HIPAS and HAARP have the ability to transmit at lower frequencies leading to pump-wave reflection and heating from resonant processes even when $f_O F2$ are below 4 MHz.

It is also possible to note from Fig. 4 that the peak ohmic energy deposition from X-mode is about four times greater than for O-mode. Therefore the effect of ohmic heating is predominantly seen in experiments with X-mode.

4 Conclusions

Observations of strong modulation of the electron temperature in the F-region by X-mode waves are reported. The thermal response of the plasma to the external heating has been examined and the rise and decay times and the magnitude of the temperature enhancements have been estimated. We have found temperature enhancements of the order of 300–400 K and characteristic times of about 10 s for the modulations. To explain these modulations we have numerically solved the electron energy equation and found that they can be well described by Ohmic heating from the pump wave. Both characteristic times and temperature enhancements are reproduced in the simulations. The observations were made during quiet night-time conditions which lead to low ionospheric densities, and therefore the radar data had to be conditionally integrated to reduce noise.

Underdense heating by X-mode is interesting in many ways, not only to test aeronomic models. Since underdense heating provides an ambient heat source without perturbing the plasma in other ways we suggest that this can be used for pre-heating the plasma to different initial temperatures for experiments investigating the temperature dependence of onset characteristics of resonant processes such as different SEE features and growth of radio induced optical emissions.

Acknowledgements. NI is supported by Swedish Research Council. EISCAT is an international association supported by research organisations in China (CRIRP), Finland (SA), France (CNRS, till end 2006), Germany (DFG), Japan (NIPR and STEL), Norway (NFR), Sweden (VR), and the United Kingdom (STFC).

Topical Editor M. Pinnock thanks two anonymous referees for their help in evaluating this paper.

References

Banks, P. M. and Kockarts, G.: Aeronomy Part B, Academic Press, London, UK; New York, USA, 1973.

Bernhardt, P. A., Tepley, C. A., and Duncan, L. M.: Airglow enhancements associated with plasma cavities formed during ionospheric heating experiments, J. Geophys. Res., 94, 9071–9092, 1989.

Brändström, B. U. E., Leyser, T. B., Steen, Å., Rietveld, M. T., Gustavsson, B., Aso, T., and Ejiri, M.: Unambigous evidence of HF pump-enhanced airglow, Geophys. Res. Lett., 26, 3561–3564, 1999.

Carlson, H. C., Wickwar, V. B., and Mantas, G. P.: Observations of fluxes of suprathermal electrons accelerated by HF excited instabilities, J. Atmos. Terr. Phys., 44, 1089–1100, 1982.

Djuth, F. T., Isham, B., Rietveld, M. T., Hagfors, T., and La Hoz, C.: First 100 ms of HF modification at Tromsø, Norway, J. Geophys. Res.-Space, 109, 11307, doi:10.1029/2003JA010236, 2004.

Gonzalez, S. A., Nicolls, M. J., Sulzer, M. P., and Aponte, N.: An energy balance study of the lower topside ionosphere using the Arecibo incoherent scatter radar and heating facilities, J. Geophys. Res., 110, A11303, doi:10.1029/2005JA011154, 2005.

Grydeland, T., Gustavsson, B., Baddeley, L., Lunde, J., and Blixt, E. M.: Conditional integration of Incoherent Scattering in relation to flickering aurora, J. Geophys. Res., 113, A08305, doi:10.1029/2008JA013039, 2008.

Gurevich, A. V.: Nonlinear effects in the ionosphere, Physics-Uspekhi, 50, 1091–1121, 2007.

Gustavsson, B., Sergienko, T., Rietveld, M. T., Honary, F., Steen, Å., Brändström, B. U. E., Leyser, T. B., Aruliah, A. L., Aso, T., and Ejiri, M.: First Tomographic estimate of volume distribution of enhanced airglow emission caused by HF pumping, J. Geophys. Res., 106, 29105–29123, 2001.

Hansen, J. D., Morales, G. J., Duncan, L., and Dimonte, G.: Large-scale HF-induced ionospheric modifications – experiments, J. Geophys. Res., 97, 113–122, 1992a.

Hansen, J. D., Morales, G. J., and Maggs, J. E.: Large-scale HF-induced ionospheric modifications – Theory and modeling, J. Geophys. Res., 97, 17019–17032, 1992b.

Hedin, A. E.: Extension of the MSIS thermosphere model into the middle and lower atmosphere, J. Geophys. Res., 96, 1159–1172, 1991.

Honary, F., Stocker, A. J., Robinson, T. R., Jones, T. B., Wade, N. M., Stubbe, P., and Kopka, H.: EISCAT observations of electron temperature oscillations due to the action of high power HF radio waves, J. Atmos. Terr. Phys., 55, 1433–1448, 1993.

Kelley, M. C., Arce, T. L., Salowey, J., Sulzer, M., Armstrong, W. T., Carter, M., and Duncan, L.: Density depletions at the 10-m scale induced by the Arecibo heater, J. Geophys. Res., 100, 17367–17376, 1995.

Kosch, M. J., Pedersen, T., Rietveld, M. T., Gustavsson, B., Grach, S. M., and Hagfors, T.: Artificial optical emissions in the high-latitude thermosphere induced by powerful radio waves: An observational review, Adv. Space Res., 40, 365–376, doi:10.1016/j.asr.2007.02.061, 2007.

Leyser, T. B.: Stimulated electromagnetic emissions by high-frequency electromagnetic pumping of the ionospheric plasma, Space Science Rev., 98, 223–328, 2001.

Leyser, T. B., Gustavsson, B., Brändström, B. U. E., Steen, Å., Honrary, F., Rietveld, M. T., Aso, T., and Ejiri, M.: Simultaneous measurements of high-frequency pump-enhanced airglow and ionospheric temperatures at auroral latitudes, Adv. Polar Upper Atmos. Res., 14, 1–11, 2000.

Mantas, G. P., Carlson, H. C., and LaHoz, C. H.: Thermal Response of the F Region Ionosphere in Artificial Modification Experiments by HF Radio Waves, J. Geophys. Res., 86, 561–574, 1981.

Pavlov, A. V.: New electron energy transfer rates for vibrational excitation of N_2, Ann. Geophys., 16, 176–182, 1998a, http://www.ann-geophys.net/16/176/1998/.

Pavlov, A. V.: New electron energy transfer and cooling rates by excitation of O-2, Ann. Geophys.-Atm. Hydr, 16, 1007–1013, 1998b.

Pavlov, A. V. and Berrington, K. A.: Cooling rate of thermal electrons by electron impact excitation of fine structure levels of atomic oxygen, Ann. Geophys., 17, 919–924, 1999, http://www.ann-geophys.net/17/919/1999/.

Ponomarenko, P. V., Leyser, T. B., and Thidé, B.: New electron gyroharmonic effects in HF scatter from pump-excited magnetic field-aligned ionospheric irregularities, J. Geophys. Res., 104, 10081–10087, 1999.

Rietveld, M., Kosch, M., Blagoveshchenskaya, N., Kornienko, V., Leyser, T., and Yeoman, T.: Ionospheric electron heating, optical emissions and striations induced by powerful HF radio waves at high latitudes: Aspect angle dependence, J. Geophys. Res., 108, 1141, doi:10.1029/2002JA009543, 2003.

Rietveld, M. T., Kohl, H., Kopka, H., and Stubbe, P.: Introduction to ionospheric heating at Tromsø– I. Experimental overview, J. Atmos. Terr. Phys., 55, 577–599, 1993.

Rishbeth, H. and van Eyken, A. P.: EISCAT – Early history and the 1st 10 years of operation, J. Atmos. Terr. Phys., 55, 525–542, 1993.

Robinson, T. R., Honary, F., Stocker, A. J., and Stubbe, P.: First EISCAT observations of the modification of F-region electron temperatures during RF heating at harmonics of the electron gyro frequency, J. Atmos. Terr. Phys., 58, 385–395, 1996.

Roble, R. G. and Hastings, J. T.: Thermal response properties of the Earth's ionospheric plasma, Planet Space Sci., 25, 217–231, 1977.

Schunk, R. W. and Nagy, A. F.: Electron temperatures in F-region of ionosphere - Theory and observations, Rev. Geophys., 16, 355–399, 1978.

Shoucri, M. M., Morales, G. J., and Maggs, J. E.: Ohmic heating of the polar F-region by HF pulses, J. Geophys. Res.-Space, 89, 2907–2917, 1984.

Showen, R. L. and Behnke, R. A.: Effect of HF-Induced plasma instabilities on ionospheric electron temperatures, J. Geophys. Res., 83, 207–209, 1978.